Available online at www.sciencedirect.com

ScienceDirect

www.elsevier.com/locate/jes

JES JOURNAL OF ENVIRONMENTAL SCIENCES

www.jesc.ac.cn

Modification of a magnetic carbon composite for ciprofloxacin adsorption

Haixin Mao, Shikui Wang, Jian-Ying Lin, Zengshuang Wang, Jun Ren*

College of Chemistry and Chemical Engineering, Key Laboratory of Coal Science and Technology, Ministry of Education and Shanxi Province, Taiyuan University of Technology, Taiyuan 030024, China. E-mail: mao5622583@163.com

ARTICLE INFO

Article history:
Received 22 February 2016
Revised 27 April 2016
Accepted 20 May 2016
Available online 15 November 2016

Keywords:
Magnetic carbon composite
Modification
Ciprofloxacin
Adsorption

ABSTRACT

A magnetic carbon composite, Fe_3O_4/C composite, was fabricated by one-step hydrothermal synthesis, modified by heat treatment under an inert atmosphere (N_2), and then used as an adsorbent for ciprofloxacin (CIP) removal. Conditions for the modification were optimized according to the rate of CIP removal. The adsorbent was characterized by Fourier transform infrared spectroscopy, X-ray diffraction measurements, vibrating-sample magnetometry, scanning electron microscopy, transmission electron microscopy, and N_2 adsorption/desorption isotherm measurements. The results indicate that the modified adsorbent has substantial magnetism and has a large specific area, which favor CIP adsorption. The effects of solution pH, adsorbent dose, contact time, initial CIP concentration, ion strength, humic acid and solution temperature on CIP removal were also studied. Our results show that all of the above factors influence CIP removal. The Langmuir adsorption isotherm fits the adsorption process well, with the pseudo second-order model describing the adsorption kinetics accurately. The thermodynamic parameters indicate that adsorption is mainly physical adsorption. Recycling experiments revealed that the behavior of adsorbent is maintained after recycling for five times. Overall, the modified magnetic carbon composite is an efficient adsorbent for wastewater treatment.

Introduction

In recent years, antibiotics have been widely used to treat bacterial infections in humans and animals. Ciprofloxacin (CIP) is a third-generation fluoroquinolone in clinical use, which has strong, wide-spectrum, antibacterial activity. CIP has been the most frequently detected antibiotic in many rivers in China because it is incompletely metabolized in humans or is released in effluent from drug manufacturing (Golet et al., 2002; Wu et al., 2010). Although the CIP concentration in the environment is low, it can induce chronic allergic reactions and antibiotic resistance in bacteria (Huang et al., 2014).

Some methods have been developed for the removal of CIP, such as ozonation (De Witte et al., 2010), photodegradation (Sturini et al., 2012), adsorption (Carabineiro et al., 2011; El-Shafey et al., 2012; Li et al., 2014; Putra et al., 2009), and biodegradation (Girardi et al., 2011). Among these methods, adsorption shows promise. This potential is due to carbon materials, which contain large surface areas, developed porous structures, rich functional groups, and a high adsorption capacity. These materials are regarded as ideal adsorbents. However, application of carbon materials is hindered by their high regeneration temperatures, low repeated-utilization ratio, difficulty of separation, and tendency for causing secondary

* *Corresponding author*. E-mail: jianyinglin@sina.com (Jian-Ying Lin).

http://dx.doi.org/10.1016/j.jes.2016.05.048
1001-0742/

pollution. Therefore, a carbon-based adsorbent that can overcome the above problems is urgently needed.

A magnetic carbon composite, Fe_3O_4/C composite, has marked advantage over traditional carbon materials because of its unique magnetic properties. It consists of an Fe_3O_4 core particle and a carbon shell. The outer carbon layer, which contains abundant functional groups such as carboxylic and hydroxyl groups, can protect the magnetic particles from degradation (Zheng et al., 2012).

By now, Fe_3O_4/C composites were synthesized through different methods (Chen et al., 2013; Shi et al., 2013; Wang et al., 2010). The adsorption capacity of Fe_3O_4/C composite for antibiotics is lower than that of the resin and carbon nanotubes (Yang et al., 2012; Bao et al., 2014; Kakavandi et al., 2013a). To improve its adsorption capacity, we prepared the composite using a hydrothermal method and modified it by treatment under an inert atmosphere (N_2) at temperatures between 450°C and 600°C. After complete characterization of the adsorbent, the effect of solution pH, adsorbent dose, contact time, CIP initial concentration, and solution temperature on the adsorption capacity were investigated. The adsorption kinetics and thermodynamics were also examined.

1. Experiment section

1.1. Materials

All chemicals used were of analytical grade. CIP was purchased from Hangzhou BaiSi Biological Technology Co., Ltd. (Hangzhou, China). Iron nitrate nonahydrate ($Fe(NO_3)_3{\cdot}9H_2O$), ferric chloride crystal ($FeCl_3{\cdot}6H_2O$), glucose, and urea were purchased from Tianjin Kermel Chemical Reagents Co., Ltd. (Tianjin, China). Distilled water was used throughout the experiments.

1.2. Preparation and surface modification of Fe_3O_4/C composite

Fe_3O_4/C composite was synthesized using a one-step hydrothermal method (Xuan et al., 2007). First, $Fe(NO_3)_3{\cdot}9H_2O$ (2.42 g) or $FeCl_3{\cdot}6H_2O$ (1.62 g), glucose (1.98 g), and urea (6.00 g) were dissolved in 40 mL of water under stirring for 10 min. The resulting solution was sealed in a 100-mL Teflon-sealed autoclave and heated to 180°C for 14 hr. After the products were cooled to room temperature, they were separated by a magnet and washed with water and ethanol five times. The products were dried at 65°C and then stored for further surface modification.

Further thermal treatments were carried out on the composites in order to modify their surface chemistry. The composites were heated to a specified temperature (450°C, 550°C, and 600°C) at a rate of 5°C/min and held at that temperature for 1 and 2 hr under an inert atmosphere (N_2). After the samples were cooled to room temperature, products were collected and treated with 1 mol/L HCl solution at 120°C for 15 min to remove the uncoated iron (Taylor et al., 2010). In the end, the sample was washed with distilled water until Cl^- could not be detected. In this article, we refer to the final dried product as the adsorbent.

1.3. Characterization of the adsorbent

X-ray diffraction (XRD) patterns of the products were obtained on a Rigaku powder diffractometer using Cu Kα radiation (λ = 0.154 nm). Scanning was done at an angle of 10°–70° at a rate of 4°/min. Fourier transform infrared (FT-IR) spectroscopy in the wavelength range of 4000–500 /cm was performed by using an FT-IR spectrometer (Shimadzu, Japan). Magnetic properties of samples were determined by vibrating-sample magnetometry (VSM, Lake Shore 7410, USA). The surface area and pore size distribution of the products were measured by nitrogen adsorption–desorption isotherm analysis at −196°C using an automatic analyzer (JW-BK, China). The morphology of the sample was investigated by scanning electron microscopy (Quanta FEG 250, USA) and transmission electron microscopy (TEM) (Tecnai F30 G^2, USA). The point of zero charge (PZC) of the adsorbent was measured through the following procedure (El-Shafey et al., 2012): Dry adsorbent (0.1 g) and CO_2-free water (20 mL) were mixed in a 100 mL Erlenmeyer flask. The flask was sealed with a cap and stirred for 48 hr. The PZC was the measured pH of the filter liquor.

1.4. Adsorption experiments

1.4.1. CIP adsorption

We carried out experiments using 250 mL glass conical flasks. Each flask contained 50 mL of CIP solution. A specified amount of adsorbent was mixed with the solution, and the resulting mixture was shaken at 130 r/min and 30°C in a shaker. The solution pH was adjusted with 0.1 mol/L HCl and 0.1 mol/L NaOH solutions. The CIP concentrations were measured by Ultraviolet–visible spectroscopy spectrophotometry at 271 nm. The adsorption capacity (q_e, mg/g) and removal rate (R, %) were calculated through Eqs. (1) and (2):

$$q_e = \frac{(C_0 - C_e)V}{w} \tag{1}$$

$$R = \frac{C_0 - C_e}{C_0} \times 100 \tag{2}$$

where C_0 (mg/L) and C_e (mg/L) are the initial and equilibrium concentrations of CIP, w (g) is the mass of the adsorbent, and V (L) is the volume of the solution.

1.4.2. Adsorption isotherms

The adsorption experiment was conducted with 0.02 g of adsorbent. The initial CIP concentration was varied from 10 to 60 mg/L. Langmuir and Freundlich models (Eqs. (3) and (4), respectively) for the adsorption isotherm were used to analyze the experimental data. Linear equations of the two isotherms for the Langmuir model are as follows:

$$\frac{C_e}{q_e} = \frac{1}{q_m b} + \frac{C_e}{q_m} \tag{3}$$

$$\ln q_e = \ln K + \frac{\ln C_e}{n} \tag{4}$$

where q_m (mg/g) is the maximum adsorption capacity, and b (L/mg) is Langmuir adsorption constant. K and n are the sorption coefficient and constant of Freundlich adsorption, respectively.

1.4.3. Adsorption kinetics

For the adsorption kinetic studies, 0.02 g of adsorbent was added to 50 mL of 10 mg/L CIP solution. The contact time ranged from 0 to 270 min. The flasks were shaken at 130 r/min at a temperature of 30°C. Pseudo first-order (Eq. (5)) and pseudo second-order (Eq. (6)) models for adsorption kinetics were used to analyze the experimental data.

$$\ln(q_e - q_t) = \ln q_e - k_1 t \tag{5}$$

$$\frac{t}{q_t} = \frac{1}{v_0} + \frac{t}{q_e} \tag{6}$$

where q_t (mg/g) is the adsorption capacity at time t, k_1 (/min) is the pseudo-first-order adsorption rate constant, and v_0 (mg/(g·min)) is the initial adsorption rate.

1.4.4. Adsorption thermodynamics

In order to understand the adsorption process, the three main adsorption thermodynamic parameters, standard free energy (ΔG^θ), standard enthalpy (ΔH^θ), and standard entropy (ΔS^θ), were calculated. The thermodynamic equilibrium constant is approximately equal to the Langmuir adsorption constant (Liu, 2009). The thermodynamic parameters were calculated through the following equations:

$$\Delta G^\theta = -RT \ln K_a \xrightarrow{K_a \approx b} \Delta G^\theta = -RT \ln b \tag{7}$$

$$\Delta G^\theta = \Delta H^\theta - T\Delta S^\theta \tag{8}$$

where R (8.314 J/(mol·K)) is the ideal gas constant, T (K) is the absolute temperature, K_a is the thermodynamic equilibrium constant (dimensionless), and b (L/mg) is the Langmuir adsorption constant. ΔG^θ was calculated from Eq. (7), and ΔH^θ and ΔS^θ were respectively obtained from the intercept and slope of the plot of ΔG^θ *versus* T.

1.5. Regeneration and recycling of the adsorbent

In order to study the regeneration of the adsorbent, 0.1 g of adsorbent was added to 50 mL of 100 mg/L CIP solution. The mixture was shaken (130 r/min) for 3 hr. After adsorption, the adsorbents were separated by an external magnetic field. The adsorbents were then added to a mixture of 10 mL of 3% NaOH solution and 50 mL methanol. The resulting mixture was shaken (130 r/min) for 30 min at 30°C. Afterwards, the adsorbents were filtered and the CIP concentration in the filter liquor was measured on a UV–Vis spectrophotometer. The above process was repeated until the CIP concentration was lower than 0.05 mg/L. Subsequently, the adsorbent was dried in an oven at 70°C for 2 hr and reused for CIP adsorption. The recycling test was carried out five times.

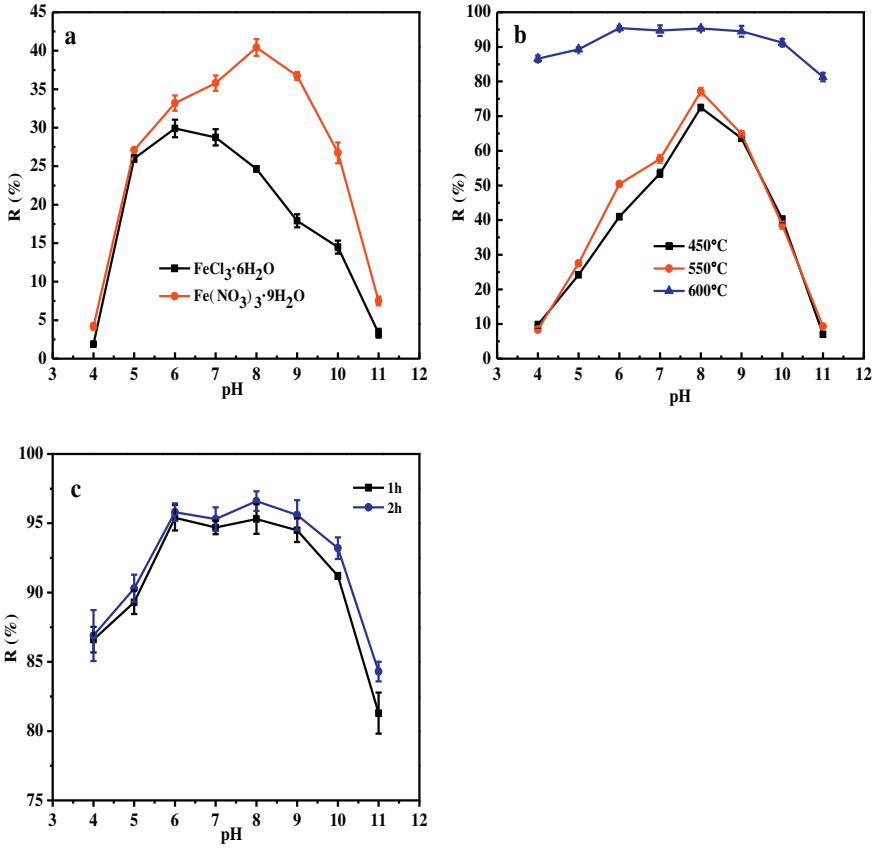

Fig. 1 – Effect of different (a) iron sources, (b) temperature [$Fe(NO_3)_3 \cdot 9H_2O$ as the iron source, thermal treat time 1 hr)] and (c) thermal treat time for the composite on adsorption removal at different pH values. Adsorption conditions: 0.02 g of adsorbent, 50 mL of 10 mg/L CIP solution, 5 hr adsorption time, and 30°C temperature. CIP: ciprofloxacin.

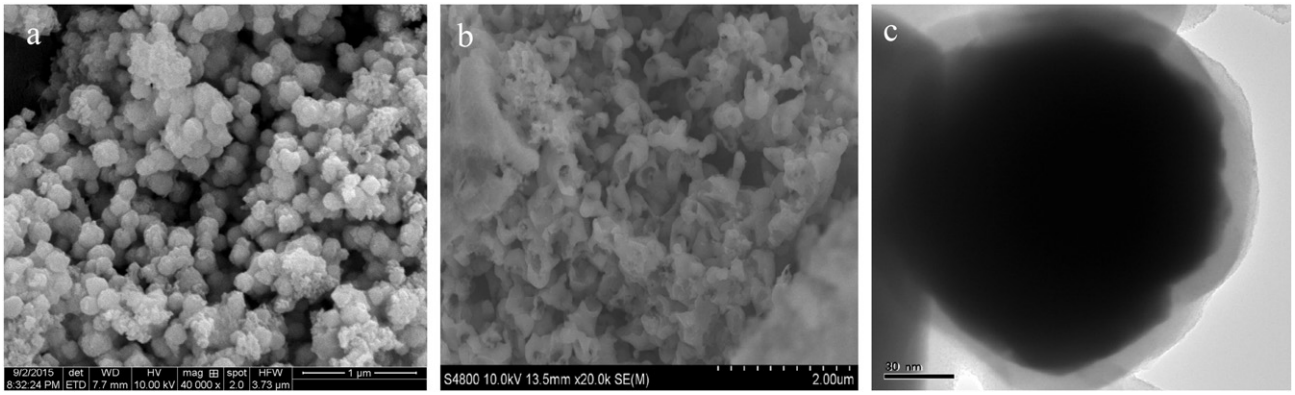

Fig. 2 – Images of Fe_3O_4/C. (a) SEM image of composite, (b) SEM: scanning electron microscopy image of adsorbent, (c) TEM image of adsorbent. TEM: transmission electron microscopy.

2. Results and discussion

2.1. *Effect of preparation conditions on the absorbability of CIP*

To optimize the preparation conditions, the effect of iron source, treatment temperature, and time on the absorbability of CIP were studied. Fig. 1a shows the rate of adsorption removal of adsorbent prepared from different iron sources at various pH values. Evidently, the composites synthesized from iron nitrate nonahydrate showed higher adsorption capacity than did those synthesized from ferric chloride. Thus, iron nitrate nonahydrate was used as the iron source. The effect of calcination temperature and time on the adsorption behavior of CIP is shown in Fig. 1b, c. According to the results, treatment at 600°C led to high CIP removal. On the other hand, the mass losses at 1 and 2 hr of thermal treatment were about 40% and 60%, respectively. On the basis of the above factors, the adsorbent synthesized from $Fe(NO_3)_3{\cdot}9H_2O$ and modified by treatment at 600°C for 1 hr was selected for subsequent adsorption experiments. The products were collected and treated with 1 mol/L HCl solution at 120 °C for 15 min. HCl treating also could increase the CIP removal rate by 2–3% compared with those untreated with HCl. This may be attributed to the dissolution of iron component, which blocked the pores' channel, in HCl solution.

2.2. *Characterization of Fe_3O_4/C composite and adsorbent*

Fig. 2a shows that the prepared Fe_3O_4/C composite is spherical, having an average size of 140 nm. The particle sizes were narrowly distributed. Fig. 2b shows that several carbon shells of the microspheres were broken after calcination and acid treatment. Such breakage may due to Fe_3O_4 loss. The TEM image in Fig. 2c indicates that Fe_3O_4 nanoparticles were coated with a carbon shell of ~10 nm thickness.

XRD patterns of the composite and adsorbent are presented in Fig. 3. According to JCPDS No. 19-0629, characteristic peaks of Fe_3O_4 crystals with a cubic structure in the composites are at 2θ values 30.1°, 35.5°, 43.0°, 53.3°, 57.0° and 62.5°, which correspond to (220), (311), (400), (422), (511) and (440) planes. For the adsorbent, characteristic peaks of Fe_3C crystals (JCPDS No.

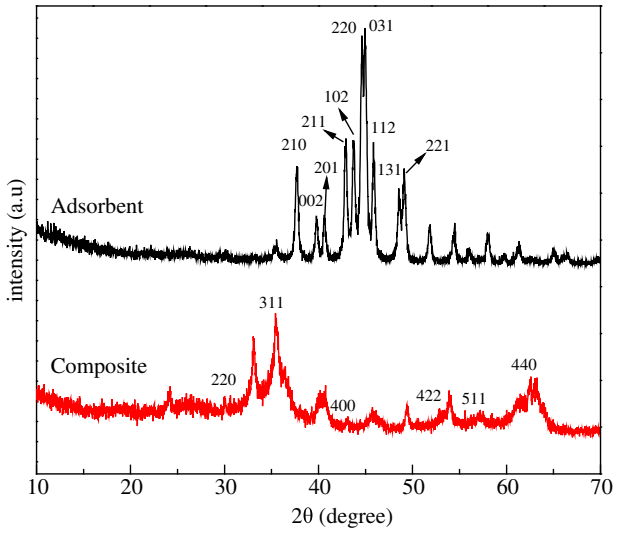

Fig. 3 – XRD patterns of composite and adsorbent. XRD: X-ray diffraction.

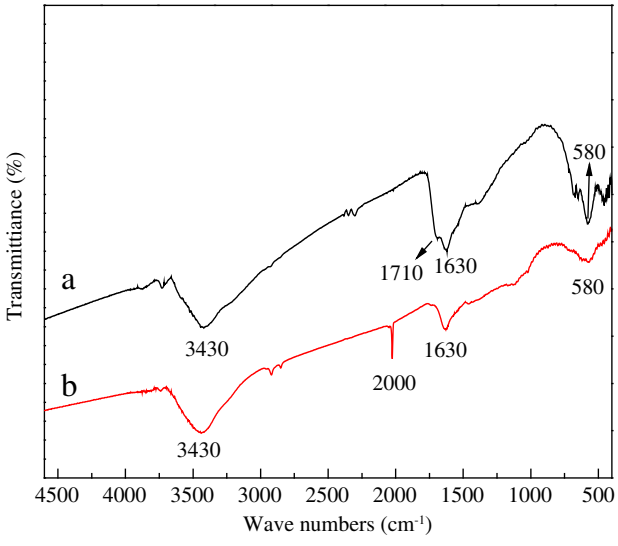

Fig. 4 – FT-IR spectra of (line a) composite and (line b) adsorbent. FT-IR: Fourier transform infrared.

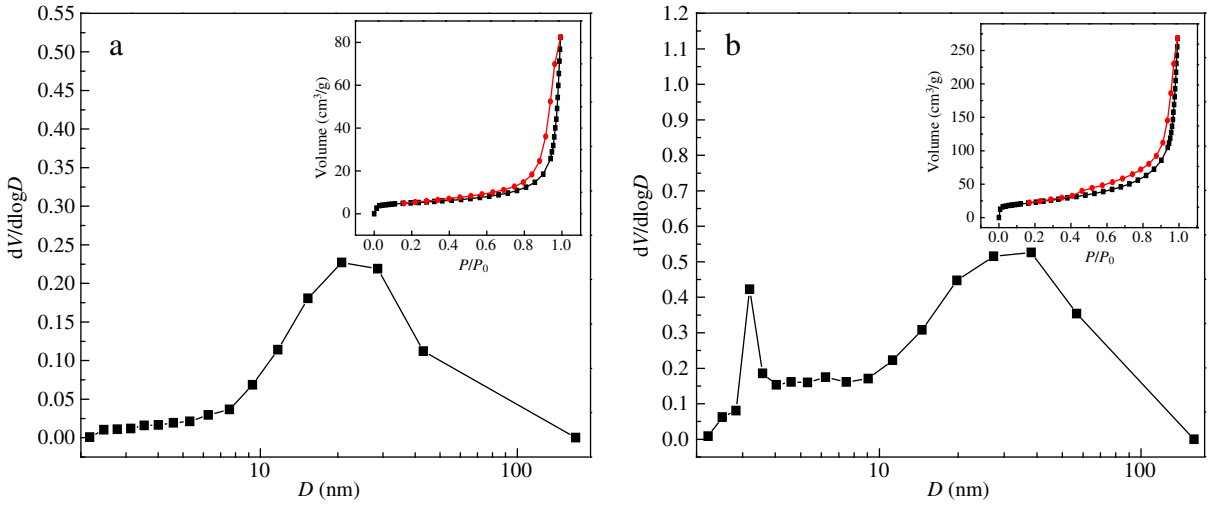

Fig. 5 – BJH: Barrett-Joyner-Halenda pore distribution and N_2 adsorption–desorption isotherms of composite (a) and adsorbent (b).

72-1110) with orthorhombic structure are at 2θ values of 37.7°, 39.8°, 40.6°, 42.9°, 43.8°, 44.6°, 44.9°, 48.6°,and 49.1°, which correspond to (210), (002), (201), (211), (102), (220), (031), (112), (131), and (221) planes. Besides, the peaks of (110) and (200) located at 44.8° and 65.2° are the characteristic peaks of Fe crystals (JCPDS No. 87-0722) with cubic structure. These results indicate that a part of the Fe_3O_4 transformed into Fe_3C and Fe. Iron components, including Fe and Fe_3O_4, have advantages toward the CIP adsorption (Jiang et al., 2015).

Fig. 4 shows FT-IR spectra of the adsorbent before and after modification. Both spectra have characteristic peaks at 3430, 1630, and 580 /cm, which represent –OH, C═C bond, and Fe–O bonds (Shi et al., 2013), respectively. Peaks at 1710 /cm (line a) imply the existence of C═O vibrations in the composite. However, the C═O bond for the adsorbent (line b) disappeared and a new characteristic peak appeared at 2000 /cm, indicating the existence of C≡C bonds on the adsorbent surface.

The pore size distribution, and N_2 adsorption/desorption isotherms of the composite and adsorbent are shown in Fig. 5. The inset in Fig. 5a and b display N_2 adsorption and desorption isotherms, respectively. Both curves have obvious hysteresis loops, which indicate that the composite and adsorbent have a mesoporous structure. Fig. 5 shows the pore distribution of the composite and adsorbent. As shown, the pore size distribution of the composite initially ranged within 20–30 nm; after modification, it was within 3–4 nm and 20–50 nm. These results suggest that calcination not only plays an important role in the expanding pore but forms a few mesopores. The Brunauer–Emmett–Teller (BET) surface areas are 17.743 and 79.017 m^2/g, clearly showing an increase after modification. Basically, specific area is a key character for an adsorbent. Larger specific area may provide more adsorptive sites, and will enhance the adsorption. Pore distribution is another important character for the adsorbent. Mesopore is in favor of mass transport, more mesopores will make CIP diffuse to the surface of the adsorbent easily, then the adsorption will be improved. Combined with the results shown in Fig. 1, it is clearly that the results proved the above point. Overall, the large surface area and porous structure seem to play an important role in CIP removal.

The magnetic properties of the adsorbent were investigated by VSM. As the saturation magnetization of the adsorbent is ~9.91 emu/g (Fig. 6), it has magnetic sensitivity. Thus, it could be separated easily. However, the saturation magnetization is lower than that of bulk Fe_3O_4 (96 emu/g) (Santiago-Rodríguez et al., 2013). This difference may be due to the existence of a carbon shell (Mao et al., 2014) and the transformation of Fe_3O_4.

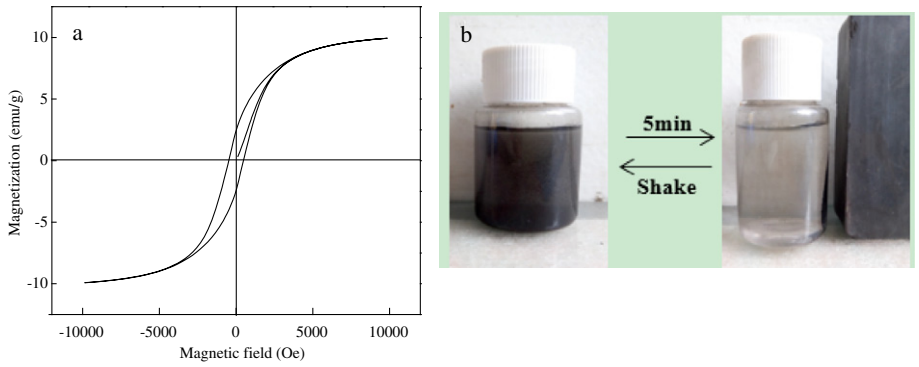

Fig. 6 – (a) Magnetization curves of the Fe_3O_4/C composite, (b) illustration of the magnetic separability of the adsorbent.

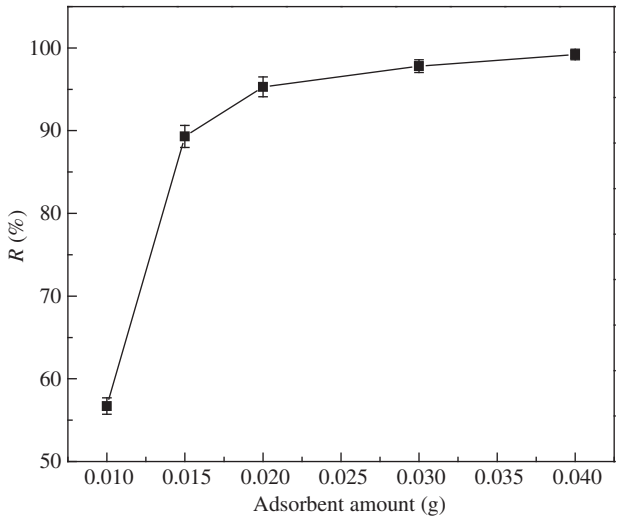

Fig. 7 – Effect of adsorbent dose for the adsorbent on adsorption removal. Adsorption conditions: 50 mL of 20 mg/L CIP solution, pH 7.0, 3 hr adsorption time, and 30°C temperature. CIP: ciprofloxacin.

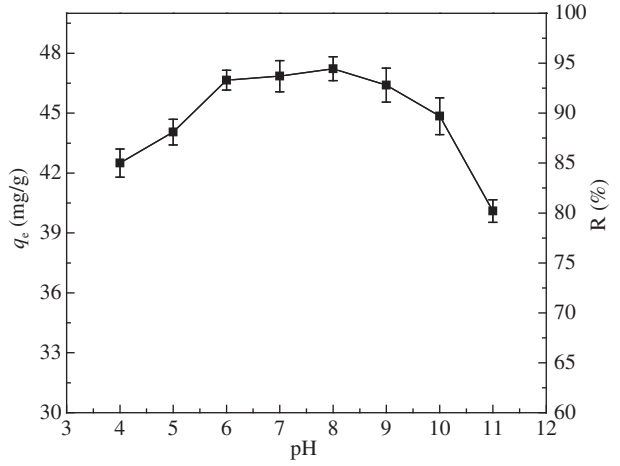

Fig. 8 – Effect of pH for the adsorbent on adsorption capacity and adsorption removal. Adsorption conditions: 0.02 g adsorbent, 50 mL of 20 mg/L CIP solution, 3 hr adsorption time, and 30°C temperature. CIP: ciprofloxacin.

2.3. Effects of the adsorbent dose and pH value on CIP removal

The influence of adsorbent dose (0.01–0.04 g) at an initial CIP concentration of 20 mg/L was tested at 30°C. As shown in Fig. 7, the results indicate that the CIP removal rate increased sharply with the increase in adsorbent dose (from 0.01 to 0.02 g) and then increased more slowly from 0.02 to 0.04 g. This result may be due to the increase in the number of adsorption sites when the amount of adsorbent increased. Therefore, 0.02 g of the adsorbent dose was used in subsequent experiments.

Fig. 8 shows the effect of pH on CIP adsorption. The results indicate a higher rate of CIP adsorption removal in the range of pH 6–9. For CIP, the acid dissociation constants are 6.1 for the carboxylic acid group (pK_{a1}) and 8.7 for the basic N moiety (pK_{a2}) (Gu and Karthikeyan, 2005). Therefore, CIP molecules mainly exist as cations because of protonation of the amine group at pH < 6.1. At pH > 8.7, CIP molecules exist as anions because of deprotonation of carboxylate. At pH in the range of 6.1–8.7, CIP molecules exist as zwitterions. Furthermore, the PZC of the adsorbent is at pH of 7.3. Therefore, when the solution is at pH < 7.3, the adsorbent surface becomes positively charged; however, at pH > 7.3, the adsorbent surface becomes negatively charged. Accordingly, electrostatic interaction between charged CIP molecules and the charged adsorbent surface at pH < 6 and pH > 9 (Fig. 8) is optimal conditions for the adsorption process. At pH at the range of 6–9, the CIP molecules and adsorbent surface have opposite charges, resulting in a high rate of adsorption removal.

As seen in Fig. 8, the adsorbent still had substantial adsorption capacity even though the rate of adsorption removal decreased at pH < 6 and pH > 9. Therefore, there may be other mechanisms leading to CIP adsorption, such as π–π interactions between the CIP molecules and adsorbent surface. The molecular structure of CIP has a benzene ring and two heterocyclic substituents. F on the benzene ring has strong electron-withdrawing ability and behaves as a π-electron acceptor. The electron donor, the carboxyl group on the adsorbent, forms π–π electron donor–acceptor pairs with CIP molecules. Therefore, the π–π electron donor–acceptor interaction may explain the adsorption process (Li et al., 2014). In addition, –OH on the adsorbent surface could form H bonds

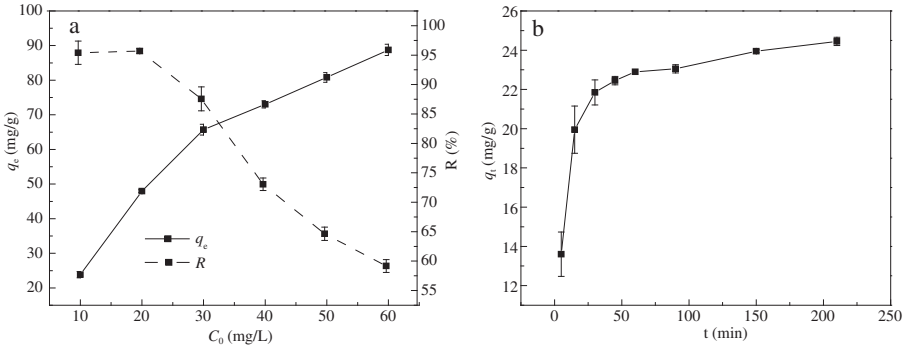

Fig. 9 – (a) Effect of initial ciprofloxacin concentration for the adsorbent on adsorption capacity and adsorption removal. Adsorption conditions: 0.02 g adsorbent, pH 7.0, 3 hr adsorption time, and 30°C temperature. (b) Adsorption kinetics of CIP with 10 mg/L CIP concentration (pH 7.0). CIP: ciprofloxacin.

Table 1 – Langmuir model and the Freundlich model parameters for adsorption of CIP.

Temperature (°C)	Langmuir			Freundlich		
	q_m (mg/g)	b (L/mg)	R^2	k	$1/n$	R^2
30	90.1	0.0917	0.9927	43.09	0.246	0.9082

R^2 is linear correlation coefficient.
CIP: ciprofloxacin.

with N-containing groups on the CIP molecules, thus improving the adsorption capacity (Kakavandi et al., 2013a). Moreover, FT-IR spectra and N_2 adsorption–desorption isotherms of the composite and adsorbent indicate that thermal treatment removes some surface groups such as C═O, which do not contribute to CIP adsorption, thereby providing more active sites for adsorption.

2.4. Adsorption isotherms and kinetics

The effect of initial CIP concentration is depicted in Fig. 9a. The CIP adsorption capacity increased with the increase in CIP initial concentration. Fig. 9a also shows that the rate of CIP removal decreased from 98% to 59.9% with the rise in initial concentration from 10 to 60 mg/L.

The adsorption isotherms were fitted by the Langmuir and Freundlich models. Corresponding calculated parameters are given in Table 1. We can observe that the Langmuir model is more suitable for describing the adsorption process than is the Freundlich model. Therefore, we can assume that CIP adsorption occurs mainly by monolayer adsorption. The theoretical maximum adsorption capacity is 90.1 mg/g at 30°C.

Fig. 9b shows the effect of contact time on CIP adsorption on the adsorbent. The adsorption rate was high during the first 50 min and subsequently decreased. There were numerous available active sites on the adsorbent surface. When the sites were occupied, the adsorption rate decreased gradually (Kakavandi et al., 2013b). Adsorption reached equilibrium at 210 min.

The pseudo first-order and pseudo second-order kinetic models were used to study the adsorption kinetics. Correlation parameters for the adsorption kinetics in the two models are shown in Table 2. As shown, CIP adsorption on the adsorbent fits the pseudo-second-order kinetics model well (R^2 = 0.99979). This fit implies that the adsorption process may be controlled by multiple factors.

Table 2 – Pseudo first- and second-order kinetics model parameters for CIP adsorption.

Kinetic model	v_o (g/(mg·min))	K (/min)	q_e (mg/g)	q_e^* (mg/g)	R^2
Pseudo first-order	–	0.018	6.824	24.3	0.92875
Pseudo second-order	0.0079	–	24.83	24.3	0.99979

q_e and q_e^* are the calculated and measured adsorption capacities of CIP, respectively.
CIP: ciprofloxacin.

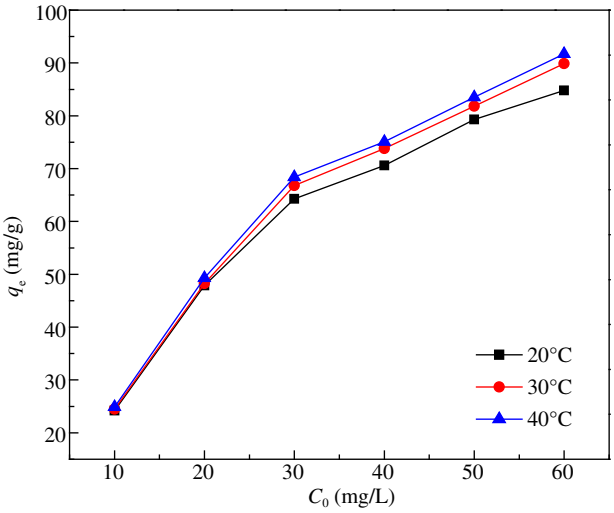

Fig. 10 – Effect of temperature for the adsorbent on adsorption capacity. Adsorption conditions: 0.02 g adsorbent, 50 mL of 20 mg/L CIP solution, 3 h adsorption time, and pH 7.0. CIP: ciprofloxacin.

2.5. Adsorption thermodynamic studies and the effect of temperature

The effect of temperature on CIP adsorption is depicted in Fig. 10. As shown in the figure, adsorption capacity increased with increasing temperature. This trend reveals that raising the temperature is advantageous to adsorption.

Results in Table 3 were obtained by calculation. We observed that ΔG^θ of adsorption is <0, whereas ΔH^θ and ΔS^θ of adsorption are >0; therefore, the adsorption process is spontaneous and endothermic. These parameters also indicate that adsorption is mainly spontaneous physical adsorption. Absolute values of the enthalpy change during physical adsorption and chemical adsorption fall within the ranges 2.1–20.9 and 80–200 kJ/mol, respectively (Sağ and Kutsal, 2000).

2.6. Effect of ion strength and humic acid

Sodium chloride was selected to investigate the effect of ion strength and the results are depicted in Fig. 11a. The results indicated that sodium chloride ranged from 0 to 12 g/L had a minor effect for the adsorbent on adsorption capacity. The Na^+ ion may compete with CIP to occupy the active adsorptive site, whereas the increase of concentration of NaCl may weaken the electrostatic interaction between adsorbent and

Table 3 – Thermodynamic parameters for adsorption of CIP.

	T (K)	b (L/mol)	ΔG^θ (kJ/mol)	R^2	ΔH^θ (kJ/mol)	ΔS^θ (kJ/mol)
Adsorbent	293	2.63×10^4	−24.7			
	303	3.03×10^4	−26.0	0.9878	13.37	130
	313	3.45×10^4	−27.3			

CIP: ciprofloxacin.

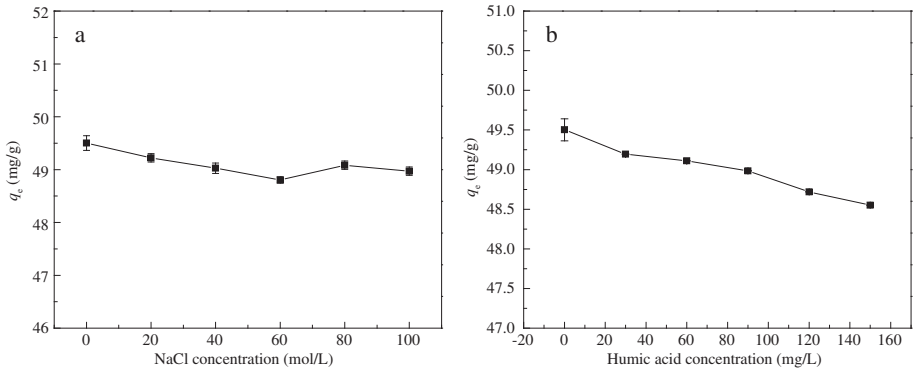

Fig. 11 – Effect of (a) ion strength and (b) humic acid for the adsorbent on adsorption capacity. Adsorption conditions: 0.02 g adsorbent, 50 mL of 20 mg/L CIP solution, 3 hr adsorption time, pH 7.0 and 30°C temperature. CIP: ciprofloxacin.

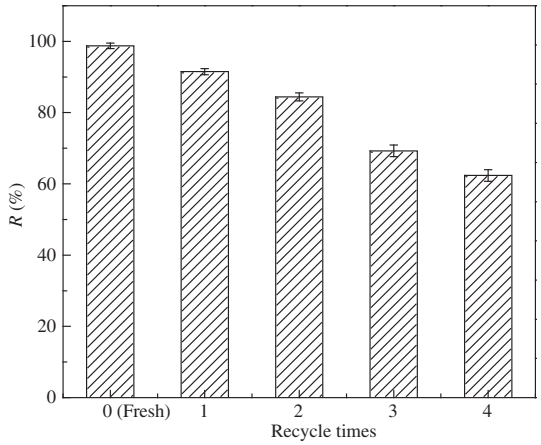

Fig. 12 – The adsorption removal rates of fresh and recycled adsorbent. Adsorption conditions: 0.1 g adsorbent, 50 mL of 100 mg/L CIP solution, pH 7.0, 3 hr adsorption time, and 30°C temperature.

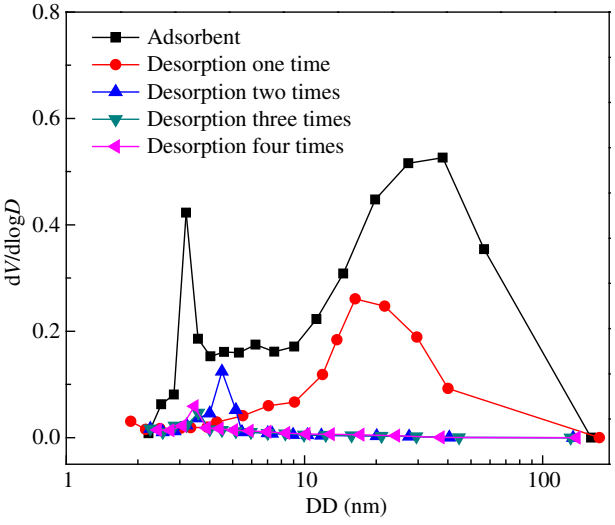

Fig. 13 – BJH: Barrett-Joyner-Halenda pore distribution of adsorbent and after desorption.

CIP due to the compression of electric double layer by NaCl. Totally, the ion strength has minor effect on the CIP adsorption capacity under the experimental condition.

Fig. 11b shows the effect of humic acid on CIP adsorption. As shown, the adsorption capacity of CIP decreased from 49.5% to 48.55% with the rose in initial humic acid concentration from 0 to 150 mg/L. The results indicated that humic acid had trifling influence for the adsorbent on adsorption capacity. This result may be due to a little adsorption of humic acid on the adsorbent surface, which occupied some active sites of adsorbent, then leading to the adsorption capacity reduced slightly.

2.7. Regeneration and recycling of adsorbent

A mixture of 10 mL 3% NaOH solution and 50 mL methanol was used to regenerate the used adsorbent. Results in Fig. 12 suggest that the removal rate decreased from 98.2% to 61.2% after five rounds of recycling. The specific areas of the recycled adsorbents had been characterized and the pores distribution had also been obtained, as shown in Fig. 13. The specific areas of the used adsorbent decreased from 79.017 to 51.042 m^2/g and the mesopores disappeared gradually with the increase of recycle times. The decrease of specific area and mesopores were inferior to absorption, so the removal rate also decreased.

2.8. Comparison with other adsorbents

Table 4 shows the adsorption capacities of CIP on various sorbents (Gu and Karthikeyan, 2005; Li et al., 2011; Shi et al.,

Table 4 – Adsorption capacities of different adsorbents.

Adsorbents	Sorption capacity (mg/g)	Reference
Fe_3O_4/C adsorbent	90.1	this work
Magnetic mesoporous carbon composite(Fe_3O_4/C)	98.3	Shi et al. (2013)
Illite	33.14	Wang et al. (2011)
Aluminum hydroxide	13.6	Gu and Karthikeyan (2005)
Kaolinite	6.62	Li et al. (2011)
Coal fly ash	1.547	Zhang et al. (2011)

2013; Wang et al., 2011; Zhang et al., 2011). It is obvious that the adsorbent in this work had a quite satisfactory adsorption capacity, which was similar to that of the magnetic mesoporous carbon composite made in different method (Shi et al., 2013). In addition, the adsorbent can be separated from aqueous solution using an external magnet and can also be regenerate and reused. Therefore, the adsorbent is a promising one for removing CIP from wastewater.

3. Conclusions

Based on the experimental results, the following conclusions are drawn.

Thermal treatment of the magnetic composite increases its specific area. As a result, its performance in CIP adsorption is markedly improved. The effect of pH of the adsorbate solution on the CIP adsorption is reduced and the magnetic property of the composite is retained after modification. These changes facilitate the application of the adsorbent. Therefore, thermal treatment is an effective method for modifying the magnetic carbon composite.

The Langmuir model is suitable for describing the adsorption process. In particular, the pseudo-second-order kinetic model fits the experimental kinetic curve well. Thus, physical adsorption is the main route of CIP adsorption on the adsorbent.

The adsorbent may be reused after it is regenerated.

Acknowledgements

This work was financial supported by the National Natural Science Foundation of China (No. 21376159), the Natural Science Foundation of Shanxi Province (No. 2013011042-2).

REFERENCES

Bao, X., Qiang, Z., Chang, J.-H., Ben, W., Qu, J., 2014. Synthesis of carbon-coated magnetic nanocomposite (Fe_3O_4@C) and its application for sulfonamide antibiotics removal from water. J. Environ. Sci. 26 (5), 962–969.

Carabineiro, S.A.C., Thavorn-Amornsri, T., Pereira, M., Figueiredo, J., 2011. Adsorption of ciprofloxacin on surface-modified carbon materials. Water Res. 45 (15), 4583–4591.

Chen, Z., Xue, Z., Chen, L., Geng, Z., Yang, R., Chen, L., Wang, Z., 2013. One-pot template-free synthesis of water-dispersive Fe_3O_4@C nanoparticles for adsorption of bovine serum albumin. New J. Chem. 37 (11), 3731–3736.

De Witte, B., Van Langenhove, H., Demeestere, K., Saerens, K., De Wispelaere, P., Dewulf, J., 2010. Ciprofloxacin ozonation in hospital wastewater treatment plant effluent: Effect of pH and H_2O_2. Chemosphere 78 (9), 1142–1147.

El-Shafey, E.-S.I., Al-Lawati, H., Al-Sumri, A.S., 2012. Ciprofloxacin adsorption from aqueous solution onto chemically prepared carbon from date palm leaflets. J. Environ. Sci. 24 (9), 1579–1586.

Girardi, C., Greve, J., Lamshöft, M., Fetzer, I., Miltner, A., Schäffer, A., Kästner, M., 2011. Biodegradation of ciprofloxacin in water and soil and its effects on the microbial communities. J. Hazard. Mater. 198, 22–30.

Golet, E.M., Alder, A.C., Giger, W., 2002. Environmental exposure and risk assessment of fluoroquinolone antibacterial agents in wastewater and river water of the Glatt Valley Watershed, Switzerland. Environ. Sci. Technol. 36 (17), 3645–3651.

Gu, C., Karthikeyan, K., 2005. Sorption of the antimicrobial ciprofloxacin to aluminum and iron hydrous oxides. Environ. Sci. Technol. 39 (23), 9166–9173.

Huang, L., Wang, M., Shi, C., Huang, J., Zhang, B., 2014. Adsorption of tetracycline and ciprofloxacin on activated carbon prepared from lignin with H_3PO_4 activation. Desalin. Water Treat. 52 (13–15), 2678–2687.

Jiang, P., Li, Y., Tong, Y., Li, J., Lan, H., Fu, M., Liu, R., 2015. Adsorption of ciprofloxacin from water using graphene oxide supported nanoscale zero valent iron. Acta Sci. Circumst. http://dx.doi.org/10.13671/j.hjkxxb.2015.0760.

Kakavandi, B., Esrafili, A., Mohseni-Bandpi, A., Jonidi, A.J., Kalantary, R.R., 2013a. Synthesis and properties of Fe_3O_4-activated carbon magnetic nanoparticles for removal of aniline from aqueous solution: equilibrium, kinetic and thermodynamic studies. Iranian J. Environ. Health Sci. Eng. 10 (1), 10–19.

Kakavandi, B., Jafari, A.J., Kalantary, R.R., Nasseri, S., Ameri, A., Esrafily, A., 2013b. Magnetic Fe_3O_4@C nanoparticles as adsorbents for removal of amoxicillin from aqueous solution. Water Sci. Technol. 69 (1), 147–155.

Li, Z., Hong, H., Liao, L., Ackley, C.J., Schulz, L.A., MacDonald, R.A., Mihelich, A.L., Emard, S.M., 2011. A mechanistic study of ciprofloxacin removal by kaolinite. Colloids Surf. B Biointerfaces 88 (1), 339–344.

Li, H., Zhang, D., Han, X., Xing, B., 2014. Adsorption of antibiotic ciprofloxacin on carbon nanotubes: pH dependence and thermodynamics. Chemosphere 95, 150–155.

Liu, Y., 2009. Is the free energy change of adsorption correctly calculated? J. Chem. Eng. Data 54 (7), 1981–1985.

Mao, G.-Y., Yang, W.-J., Bu, F.-X., Jiang, D.-M., Zhao, Z.-J., Zhang, Q.-H., Fang, Q.-C., Jiang, J.-S., 2014. One-step hydrothermal synthesis of Fe_3O_4@C nanoparticles with great performance in biomedicine. J. Mater. Chem. B 2 (28), 4481–4488.

Putra, E.K., Pranowo, R., Sunarso, J., Indraswati, N., Ismadji, S., 2009. Performance of activated carbon and bentonite for adsorption of amoxicillin from wastewater: mechanisms, isotherms and kinetics. Water Res. 43 (9), 2419–2430.

Sağ, Y., Kutsal, 2000. Determination of the biosorption heats of heavy metal ions on *Zoogloea ramigera* and *Rhizopus arrhizus*. Biochem. Eng. J. 6 (2), 145–151.

Santiago-Rodríguez, L., Lafontaine, M.M., Castro, C., Méndez-Vega, J., Latorre-Esteves, M., Juan, E.J., Mora, E., Torres-Lugo, M., Rinaldi, C., 2013. Synthesis, stability, cellular uptake, and blood circulation time of carboxymethyl-inulin coated magnetic nanoparticles. J. Mater. Chem. B 1 (22), 2807–2817.

Shi, S., Fan, Y., Huang, Y., 2013. Facile low temperature hydrothermal synthesis of magnetic mesoporous carbon nanocomposite for adsorption removal of ciprofloxacin antibiotics. Ind. Eng. Chem. Res. 52 (7), 2604–2612.

Sturini, M., Speltini, A., Maraschi, F., Pretali, L., Profumo, A., Fasani, E., Albini, A., Migliavacca, R., Nucleo, E., 2012. Photodegradation of fluoroquinolones in surface water and antimicrobial activity of the photoproducts. Water Res. 46 (17), 5575–5582.

Taylor, A., Krupskaya, Y., Costa, S., Oswald, S., Krämer, K., Füssel, S., Klingeler, R., Büchner, B., Borowiak-Palen, E., Wirth, M.P., 2010. Functionalization of carbon encapsulated iron nanoparticles. J. Nanopart. Res. 12 (2), 513–519.

Wang, H., Sun, Y.-B., Chen, Q.-W., Yu, Y.-F., Cheng, K., 2010. Synthesis of carbon-encapsulated superparamagnetic colloidal nanoparticles with magnetic-responsive photonic crystal property. Dalton Trans. 39 (40), 9565–9569.

Wang, C.J., Li, Z., Jiang, W.T., 2011. Adsorption of ciprofloxacin on 2:1 dioctahedral clay minerals. Appl. Clay Sci. 53 (4), 723–728.

Wu, Q., Li, Z., Hong, H., Yin, K., Tie, L., 2010. Adsorption and intercalation of ciprofloxacin on montmorillonite. Appl. Clay Sci. 50 (2), 204–211.

Xuan, S., Hao, L., Jiang, W., Gong, X., Hu, Y., Chen, Z., 2007. A facile method to fabricate carbon-encapsulated Fe_3O_4 core/shell composites. Nanotechnology 18 (3), 035602.

Yang, W., Lu, Y., Zheng, F., Xue, X., Li, N., Liu, D., 2012. Adsorption behavior and mechanisms of norfloxacin onto porous resins and carbon nanotube. Chem. Eng. J. 179, 112–118.

Zhang, C.L., Qiao, G.L., Zhao, F., Wang, Y., 2011. Thermodynamic and kinetic parameters of ciprofloxacin adsorption onto modified coal fly ash from aqueous solution. J. Mol. Liq. 163 (1), 53–56.

Zheng, J., Liu, Z., Zhao, X.S., Liu, M., Liu, X., Chu, W., 2012. One-step solvothermal synthesis of Fe_3O_4@C core–shell nanoparticles with tunable sizes. Nanotechnology 23 (16), 165601.